Chemical Engineering Journal 176–177 (2011) 280–285

Contents lists available at ScienceDirect

Chemical Engineering Journal

journal homepage: www.elsevier.com/locate/cej

Ethanol steam reforming over cobalt talc in a plate microreactor

M. Domínguez[a,b], G. Cristiano[a], E. López[a,c], J. Llorca[a,b,*]

[a] Institut de Tècniques Energètiques, Universitat Politècnica de Catalunya, Diagonal 647, Ed. ETSEIB, 08028 Barcelona, Spain
[b] Centre for Research in Nanoengineering, Universitat Politècnica de Catalunya, Pasqual i Vila 15, Ed. ETSEIB, 08028 Barcelona, Spain
[c] Planta Piloto de Ingeniería Química (CONICET-UNS), Camino de la Carrindanga km 7, 8000 Bahía Blanca, Argentina

ARTICLE INFO

Article history:
Received 26 November 2010
Received in revised form 11 January 2011
Accepted 23 March 2011

Keywords:
Hydrogen
Reforming
Ethanol
Catalytic wall
Microreactor

ABSTRACT

Stainless steel plates were coated with cobalt talc ($Co_3[Si_2O_5]_2(OH)_2$) and used in a catalytic plate microreactor for producing hydrogen from ethanol steam reforming at low temperature. Cobalt talc was deposited successfully by one-step hydrothermal synthesis from $Co(NO_3)_2{\cdot}6H_2O$ and Na_2SiO_3 at 463 K for 60 h and characterized by scanning electron and confocal microscopy, X-ray diffraction, infrared spectroscopy, and mechanical stability tests. Catalytic plates did not require any activation treatment and showed fast start-up. At 648 K and $W/F_{EtOH} = 0.5$ g min mol^{-1} complete ethanol conversion was attained and the yield to the reforming products, H_2 and CO_2, was 97 and 90%, respectively, whereas CO was detected at a trace level (<0.1%).

1. Introduction

The growth in the last years of the market for power sources for new portable devices has moved researchers to investigate in the development of miniaturized fuel cell systems. Most low-temperature fuel cell types require hydrogen for their operation and, consequently, numerous technologies are under investigation for on-site hydrogen generation from various liquid fuels as an alternative to direct hydrogen storage [1,2]. Among them, ethanol is particularly appealing since it is a renewable source when obtained from biomass, it is easy to handle and distribute and it is readily available [3]. In recent years, numerous catalyst formulations have been studied intensively for ethanol steam reforming aiming at the generation of hydrogen [4–6]:

$$C_2H_5OH + 3H_2O \rightarrow 6H_2 + 2CO_2$$

However, one of the major drawbacks of fuel processors is the difficulty to get rapid start-up and fast transient operation [7]. For that reason, monolithic reactors and plate heat-exchangers as well as microreaction technologies are preferred [8], although even in these cases it is not feasible to achieve start-up times less than several minutes before stable operation, which is unacceptable for most portable applications. Two reasons mainly account for slow start-up of current fuel processors. First, several catalytic stages with different heat requirements are necessary for obtaining a hydrogen-rich reformate with low CO concentration for feeding low-temperature fuel cells. These catalytic stages include fuel reforming, water–gas shift and CO clean-up. Second, most catalysts need an activation treatment prior to operation, which in the case of small fuel processors is a serious drawback since air exposure is expected both during start-up and shut-down periods.

One way to overcome these limitations is to develop fuel reformers containing catalysts able to efficiently reform fuels at low temperature, in such a way that the water–gas shift reaction is thermodynamically favored and occurs simultaneously with steam reforming and, consequently, CO concentration is kept low. These conditions would considerably simplify the fuel processor design, both in terms of number of catalytic stages required as well as heat transfer management. For the steam reforming of ethanol, the most active and selective to H_2 and CO_2 at low temperature are cobalt-based catalysts, which usually operate at 673–823 K [9–24]. CO contents as low as 1.5% in the reformate have been obtained, for example, over a Co-Fe/ZnO catalyst at 673 K for $W/F_{EtOH} = 10^3$ g min mol^{-1} and steam to carbon ratio (S/C) of 4 [21]. In the last years, we have studied at the Technical University of Catalonia the catalytic performance of structured reactors and microreactors coated with cobalt catalysts for ethanol processors [25–33]. We have found that cordierite monoliths loaded with cobalt talc ($Co_3[Si_2O_5]_2(OH)_2$) perform excellent for the above-mentioned reaction, both in terms of operation temperature and fast start-up [28]. At a temperature considerably lower than those reported previously for ethanol steam reforming, namely 623 K, a reformate composition of 68.7% H_2, 23.2% CO_2, 1.0% CO and 7.1% CH_4 is measured at S/C = 1.5 (stoichiometric ethanol–water mix-

* Corresponding author at: Institut de Tècniques Energètiques, Universitat Politècnica de Catalunya, Av. Diagonal 647, Ed. ETSEIB, 08028 Barcelona, Spain. Tel.: +34 93 401 17 08; fax: +34 93 401 71 49.
E-mail address: jordi.llorca@upc.edu (J. Llorca).

1385-8947/$ – see front matter © 2011 Elsevier B.V. All rights reserved.
doi:10.1016/j.cej.2011.03.087

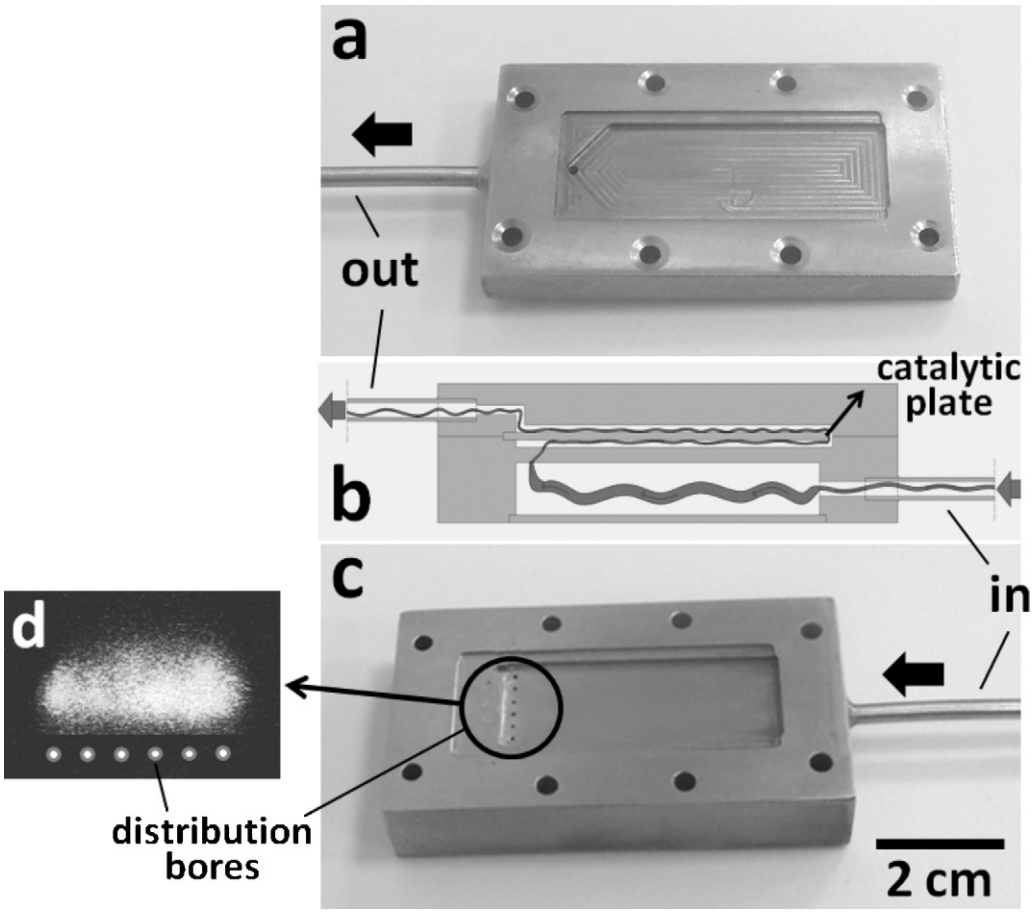

Fig. 1. Stainless steel machined microreactor used to perform reaction tests over the functionalized metal plates. (a) Photograph of the top halve of the reactor with outlet conduit and flow channel. (b) Schematic representation of the assembled microreactor with flow path. The catalytic plate is placed between both halves and the preheating/distribution chamber is shown below. (c) Photograph of the bottom halve, with inlet conduit and detail of the distribution bores. (d) Snapshot of hydrogen combustion to verify homogeneous distribution in the channel width.

ture) and ethanol full conversion [28]. This low CO concentration in the reformate stream can be directly removed by preferential oxidation, thus avoiding additional water–gas shift units. In addition, the catalyst exhibits fast start-up (few seconds) and a stable reformate composition is obtained, even after shut-down and exposure to air up to 613 K. We have shown recently that cobalt talc undergoes delamination into individual nanolayers under reaction conditions and, simultaneously, metal cobalt ensembles segregate at the surface of the nanolayers, thus offering a composite material with high surface area and reactivity, which accounts for the outstanding catalytic behavior observed [34]. Given its potential use for on-site hydrogen generation in ethanol processors for fuel cell feeding in portable applications, here we describe the preparation of cobalt talc over stainless steel plates to improve heat transfer in fuel reformers and a study of their performance for producing hydrogen in a microreactor at different temperatures and residence times.

2. Experimental

2.1. Preparation of catalytic plates

Stainless steel plates measuring 50 mm × 20 mm × 1 mm were used as a catalyst support. ($Co_3[Si_2O_5]_2(OH)_2$) was grown over the metal plates by a hydrothermal method [35]. $Co(NO_3)_2{\cdot}6H_2O$ and Na_2SiO_3 (Co:Si = 1:4 molar) were mixed in ethanol–water (H_2O:C_2H_5OH = 1:4 vol.) and placed in a 100 mL Teflon vessel containing the metal plate vertically inside a batch reactor. Since there are no reports in the literature concerning the deposition of talc phases over metal supports, the effect of hydrothermal temperature (423–463 K) and time (5–60 h) were explored. Also, the effect of pickling (NaOH 20 M at 363 K for 30 min) over the metal plates to enhance roughness prior to hydrothermal synthesis was evaluated. After the hydrothermal reaction, catalytic plates were rinsed with abundant deionized water in order to remove non-bonded solid and used for catalytic tests without further treatment.

2.2. Characterization techniques

Three-dimensional, non-invasive assessment of the microgeometry of the catalyst layer over the stainless steel plates was performed by confocal microscopy with a Veeco Wyko NT9300 surface profiler apparatus. The catalytic plates were scanned at a step height of ca. 10 μm/s, and the total height analyzed was about 40 μm. Surface roughness is given by the average roughness value, R_a, which is the arithmetic mean of the departure of the profile from the center line of a line scan of the surface. Mechanical stability was evaluated by two different methods. In one method, the catalytic plates were immersed in water and exposed to high frequency ultrasounds (40 kHz) and the weight loss was monitored for 15 min. In the second method, catalytic plates were exposed directly to mechanical vibration. The acceleration value was raised progressively from 5 to 20 G and weight loss was monitored after 30 min at each acceleration value. The microstructure, morphology, and composition of the catalyst layer were studied with a Zeiss NEON40 crossbeam scanning electron microscope (SEM) operated

at 5 kV and equipped with energy dispersive X-ray analysis (EDX) and focus ion beam (FIB). Grazing angle X-Ray diffraction (XRD) measurements were performed with a Bruker d8 Advance diffractometer (CuKα incident radiation). XRD profiles were recorded from 5° to 70° (2θ) at a step size of 0.02°, step time of 6 s, and fixed incident angle of 1–3°. Grazing angle infrared spectroscopy (FTIR) was performed with a SMART SAGA platform mounted in a Nicolet 6700 infrared spectrometer at a fixed incidence angle of 80°. FTIR spectra were obtained by accumulating 64 scans in the range of 600–4000 cm^{-1} with a resolution of 4 cm^{-1}.

2.3. Reaction tests

The functionalized plates described above were implemented in a microreactor machined in stainless steel in two differentiated halves, as shown in Fig. 1. Each reactor halve comprised a 0.5 mm-height rectangular cavity which constituted the flow channel (Fig. 1a and c). The catalytic plate was sandwiched between the two halves, except at one of the ends where a window communicated upper and lower flow channels. High temperature sealing paste was used to avoid lateral by-passes from one side to the other of the catalytic plate. By these means, the reacting mixture flowed axially along both sides of the plate, as schematized in Fig. 1b. The lower part of the reactor (Fig. 1c) comprised distribution and preheating facilities. A gas chamber offered an enhancement of the residence time of the incoming feed to achieve the desired reaction temperature. Six equidistant 0.5 mm-diameter bores were implemented between the preheating chamber and the lower flow channel to assure a uniform distribution of the feed on the channel width. Hydrogen combustion was used to verify an adequate flow distribution through the bores, as shown in the snapshot in Fig. 1d. Stainless steel screws were employed to assemble the microreactor and additional sealing paste was used between the two reactor halves to avoid gas leakage. The whole reaction unit was disposed inside an electrical furnace to reach the reaction temperature. K-type thermocouples (±0.5 K) were placed in contact with the microreactor and in the gas outlet to control the furnace temperature. The whole microreactor measured 70 mm × 40 mm × 19 mm.

Catalytic tests were carried out at atmospheric pressure in the temperature range 598–773 K. A C_2H_5OH:H_2O = 1:6 (molar) vapor mixture balanced with inert gas was passed through the reactor at 30–70 STP mL min^{-1} (0.3–0.8 mL min^{-1} C_2H_5OH). Prior to catalytic tests, the temperature of the microreactor was raised up to 598 K in air and held at this temperature for 30 min. The reactor effluent was monitored continuously by on-line gas chromatography (Agilent 3000A) using MS 5 Å, PlotU and Stabilwax columns. Blank runs at 473–773 K showed negligible ethanol conversion.

3. Results and discussion

3.1. Catalytic plates

To study the effect of the hydrothermal temperature on the formation of cobalt talc over the stainless steel plates, several synthesis were carried out between 423 and 463 K. Also, the effect of time of the hydrothermal treatment, which is an important parameter in hydrothermal synthesis, was evaluated by performing experiments between 5 and 60 h. Fig. 2 shows representative scanning electron microscopy images recorded directly over coated stainless steel plates. The catalytic layer obtained at 423 K for 5 h (Fig. 2a) is comprised by crystallites of about 200–300 nm in size with a clear cubic crystalline habit. Energy-dispersive analysis (EDX) reveals that those crystallites only contain cobalt and oxygen, and X-ray diffraction (XRD) shows peaks at 19.0, 31.3, 36.9, 44.8, 59.3 and 65.2°, which are characteristic of (1 1 1), (2 2 0), (3 1 1), (4 0 0), (5 1 1) and (4 4 0) crystallographic planes of cobalt spinel (Co_3O_4), respectively. In contrast, the catalytic layer obtained at 463 K for 5 h (Fig. 2b) exhibits particles with a pseudo-layered structure. EDX analysis shows the presence of silicon in addition to cobalt and oxygen, and in the XRD pattern there is a characteristic peak at 9.3° of the cobalt talc structure, which corresponds to the (0 0 1) basal crystallographic plane [36]. The catalyst coating formed at the same temperature, 463 K, but after 60 h of hydrothermal synthesis

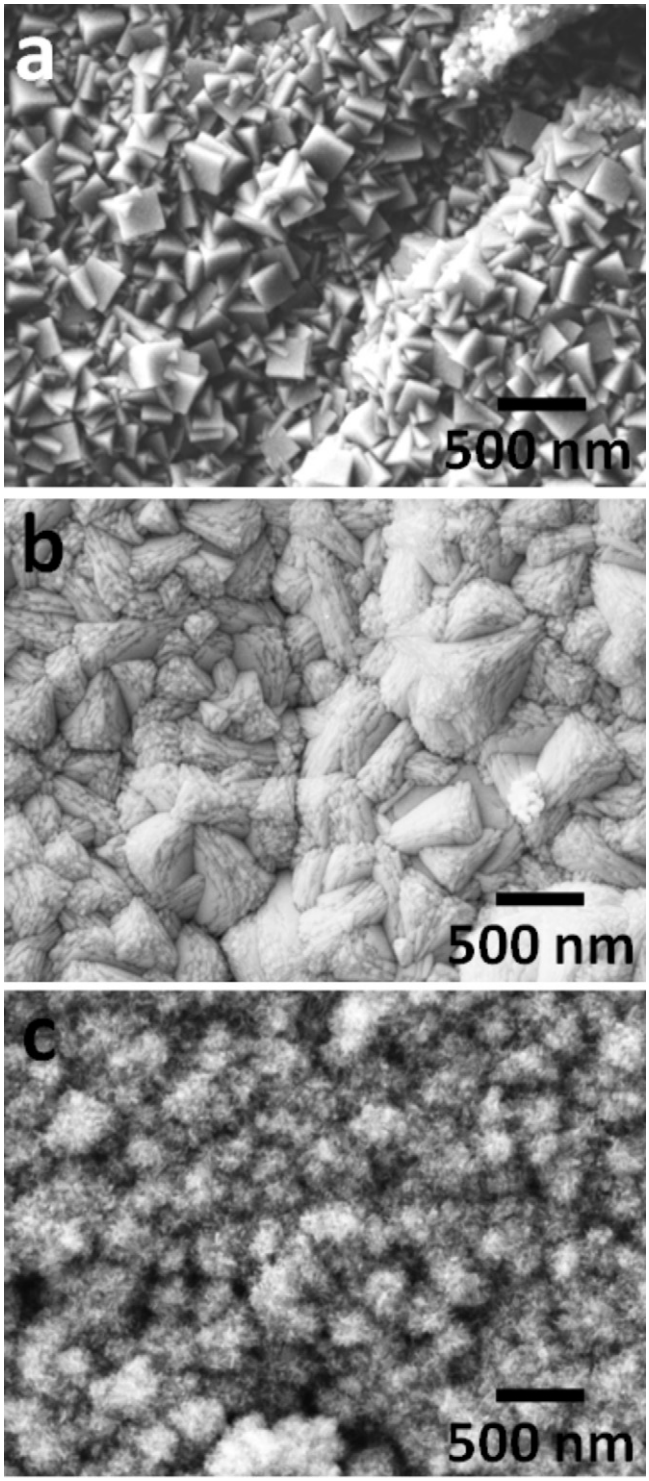

Fig. 2. Scanning electron microscopy (SEM) images recorded at the same magnification of catalyst coatings over stainless steel plates after hydrothermal synthesis at 423 K for 5 h (a), 463 K for 5 h (b), and 463 K for 60 h (c).

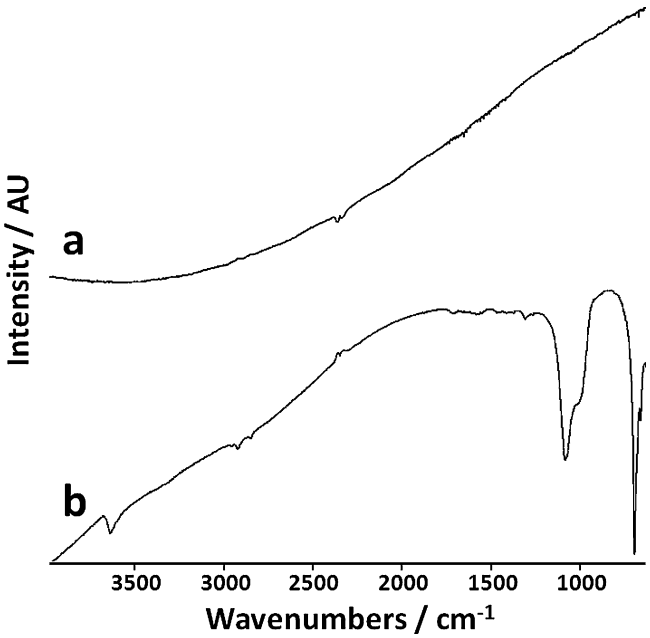

Fig. 3. Grazing angle FTIR spectra of a stainless steel plate before (a) and after (b) hydrothermal synthesis at 463 K for 60 h.

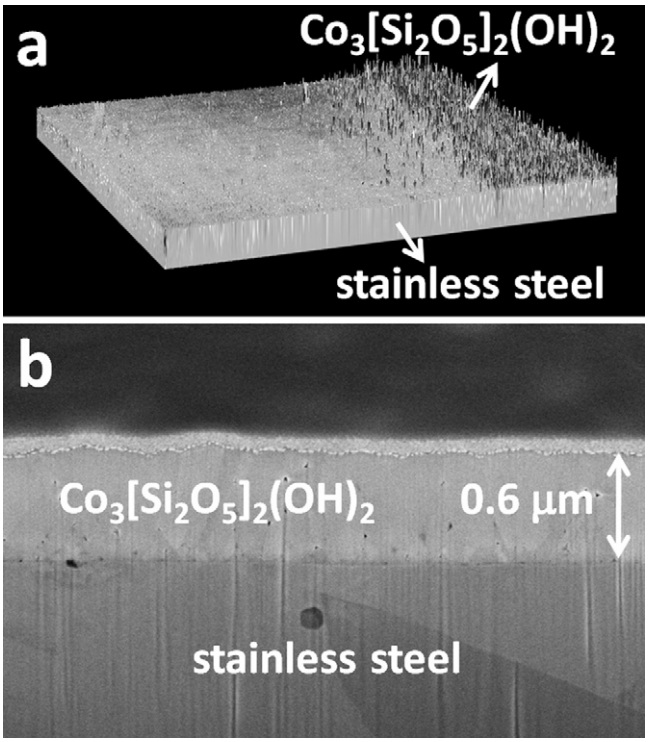

Fig. 4. (a) Confocal microscopy image of a stainless steel plate partially covered by a layer of cobalt talc. (b) SEM image of the catalyst layer after cutting with an ion beam (FIB).

(Fig. 2c) contains cobalt talc particles that are much smaller, about 10–20 nm in length, indicating that both the hydrothermal temperature and time are key parameters for obtaining catalyst coatings with well-formed and well-dispersed cobalt talc particles. Therefore, the catalytic stainless steel plates used for catalytic tests in this work were obtained at 463 K for 60 h. Fig. 3 shows raw grazing angle infrared reflection spectra of a bare stainless steel plate (Fig. 3a) and a plate coated with cobalt talc by hydrothermal synthesis at 463 K for 60 h (Fig. 3b). Bands at 3640, 1020 and 680 cm^{-1} are characteristic of OH stretching, Si—O stretching and Si—O—Co bending vibrations of cobalt talc [37,38].

The thickness of the cobalt talc layer over the stainless steel plates was measured by confocal microscopy and SEM. A hydrothermal synthesis was performed at 463 K for 60 h maintaining only approximately half of the metal plate immersed in the solution. Then, the uncoated and coated intermediate zone was imaged by confocal microscopy. Fig. 4a shows a representative image of an intermediate zone measuring ca. 10 mm^2. As expected, the area coated with catalyst exhibits a higher roughness ($R_a \sim 0.54$) than that of the uncoated area ($R_a \sim 0.37$) due to an enhancement of surface area ascribed to the small layers of cobalt talc. The mean thickness of the catalytic layer is about 0.5 μm. Fig. 4b is a SEM image recorded over the coated zone after cutting the catalyst layer with an ion beam (FIB). The cut is oriented perpendicular to the catalytic layer and was performed after sputtering with Pt in order to get a sharp edge (bright thin layer in the image). The mean thickness of the catalytic layer measured by this technique is about 0.6 μm, which is fairly similar than that calculated by confocal microscopy. Mechanical stability of the catalyst coating was evaluated as well. No weight loss was measured after 30 min of exposure to 20 G mechanical vibration, and after 15 min of exposure to ultrasounds a negligible weight loss of <0.1% was detected. Therefore, the catalytic plates prepared in this work fulfill the stability requirements of fuel reformers in portable applications, where loss of catalytic coatings should be completely avoided to prevent downstream plugging and loss of activity. No further enhancement of the cobalt talc layer adherence over the stainless steel plates was observed following pickling treatments of the stainless steel support.

A study of catalyst loading was also carried out in order to prepare catalytic plates with different amount of catalyst towards reaction tests. This was accomplished by varying the concentration of reactants in the hydrothermal synthesis. Fig. 5 shows a plot of cobalt talc loading with respect to concentration of cobalt precursor used in several experiences, maintaining a constant Co/Si molar ratio of 0.25. In the range of concentrations studied, there is a linear trend between catalyst loading and reactant concentration. This means that stainless steel plates can be coated with appropriate amount of cobalt talc in a single preparation hydrothermal step.

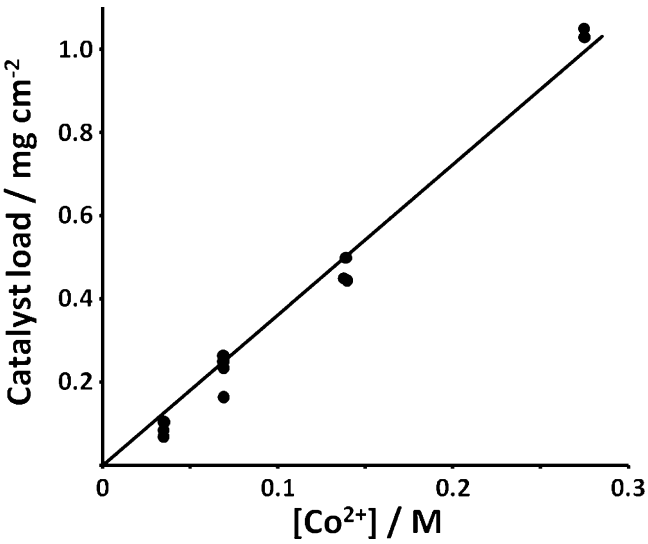

Fig. 5. Plot of cobalt talc loading onto stainless steel plates obtained by hydrothermal synthesis at 463 K for 10 h under different concentration of reactants.

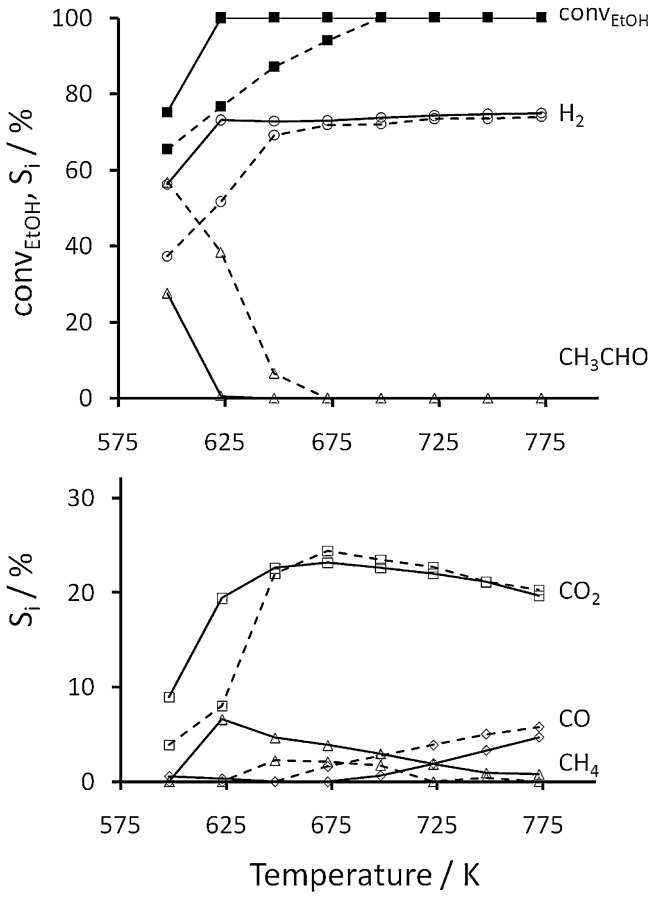

Fig. 6. Ethanol conversion and product distribution on a dry basis obtained over stainless steel plates loaded with 1 mg cm^{-2} (dashed lines) and 3 mg cm^{-2} (solid lines) of cobalt talc. τ_{STP} = 30 ms, S/C = 3, 0.5 mL min^{-1} C_2H_5OH, P_{atm}.

3.2. Ethanol steam reforming

Two sets of experiments were carried out over two different stainless steel plates loaded with 1 and 3 mg cobalt talc cm^{-2} without any activation pretreatment. In the first set, a constant feed of ethanol–water (S/C = 3, 0.5 mL min^{-1} C_2H_5OH, τ_{STP} = 30 ms) was passed over the catalytic plates and the temperature was raised progressively from 598 to 773 K. In the second set of experiments, the contact time was varied from τ_{STP} = 20 to 50 ms at constant temperature of 623 K and using a fixed reactants inlet concentration.

Fig. 6 shows the performance attained by both catalytic plates loaded with different amount of cobalt talc at the different temperatures tested. For the catalytic plate with 3 mg cm^{-2}, ethanol conversion is total at 623 K and above (solid line), whereas over the catalytic plate with 1 mg cm^{-2} a temperature of 698 K is required to complete ethanol transformation (dashed line). The amount of hydrogen evolved in both cases with increasing temperature follows the transformation of ethanol. Acetaldehyde is present among the reaction products at low temperature, specially over the catalytic plate with 1 mg cm^{-2}, and vanishes rapidly as the reaction temperature increases, in accordance to a reaction scheme where ethanol first dehydrogenates at low temperature into acetaldehyde and hydrogen, and then acetaldehyde is reformed with steam into H_2 and CO_2 [28]. Thus, in both catalytic plates the selectivity of hydrogen and carbon dioxide, the reforming products, increase sharply at the expenses of acetaldehyde (Fig. 6). It is noteworthy that the product distribution reached by both catalytic plates is fairly similar at high temperature and that the only major difference relies on the temperature required to complete ethanol and acetaldehyde conversions due to the different catalyst loading. However, the amount of carbon monoxide is higher when the reaction is performed over the catalytic plate with low catalyst loading. This is explained in terms of a reaction scheme with consecutive reactions. In addition to steam reforming, the water gas shift reaction (WGS) is also operative over cobalt talc and the CO produced by decomposition reactions is transformed into CO_2 more efficiently over the catalytic plate with higher catalyst loading under the same contact time. In both cases, the increase in CO concentration and the concomitant decrease of CO_2 at the reactor outlet when the temperature is increased is an expected consequence of the WGS thermodynamics. Over the catalytic plate with 3 mg cobalt talc cm^{-2} and at low temperature (648–673 K) a reformate composition of ca. 73% H_2, 23% CO_2 and 4% CH_4 is measured at ethanol full conversion, with CO levels below 0.01%. At 773 K the composition of the reformate (74.9% H_2, 19.7% CO_2, 0.8% CH_4 and 4.7% CO) approaches equilibrium values (71.8% H_2, 20.8% CO_2, 1.8% CH_4 and 5.7% CO).

The effect of contact time is similar in both catalytic plates. Operating at 623 K, a decrease in contact time down to 20 ms leads to kinetic limitations, as evidenced by an increase of both acetaldehyde and CO at the reactor outlet (up to 19 and 5.5%, respectively, for the catalytic plate with 3 mg cobalt talc cm^{-2}). Conversely, an increase of contact time up to 50 ms favors the WGS reaction and acetaldehyde is completely reformed as well as ethanol. It is deduced that both the reaction temperature and contact time have a strong influence on the catalytic performance and that both parameters need to be properly adjusted for maximizing the hydrogen yield while maintaining CO at low levels.

4. Conclusions

Aiming at a low-temperature ethanol reforming catalyst supported over a carrier with good heat transfer properties, cobalt talc has been successfully loaded onto stainless steel plates by a one-step hydrothermal route. Homogeneous catalytic layers with a thickness less than 1 μm and excellent adherence are obtained at 463 K after 60 h of hydrothermal synthesis. The coating is constituted by cobalt talc nanoparticles of 10–20 nm in size. The performance of the functionalized metal plates towards the endothermic steam reforming of ethanol (ESR) for producing hydrogen at low temperature has been tested in a specifically designed microreactor. It has been demonstrated that the catalytic plates are active for ESR and do not require any treatment prior to reaction, thus indicating that this type of device is of interest for the development of ethanol fuel processors for portable applications. In addition, low amounts of CO are encountered at the reactor outlet at 648–673 K for W/F_{EtOH} values above 0.5 g min mol^{-1}, which may be abated directly by preferential oxidation without the requirement of additional WGS units.

Acknowledgements

This work has been funded through MICINN grant CTQ2009-12520. M.D. acknowledges an FI grant from Generalitat de Catalunya and European Social Fund. J.L. is grateful to ICREA Academia program.

References

[1] R.M. Navarro, M.A. Peña, J.L.G. Fierro, Catal. Rev. 107 (2007) 3952.
[2] J. Llorca, Microreactors for the generation of hydrogen from ethanol, in: W.H. Lee, V.G. Cho (Eds.), Handbook of Sustainable Energy, Nova Publishers, 2010, pp. 693–699, Chapter 22.
[3] H. Idriss, M. Scott, J. Llorca, S.C. Chan, W. Chiu, P.Y. Sheng, A. Yee, M.A. Blackford, S.J. Pas, A.J. Hill, F.M. Alamgir, R. Rettew, C. Petersburg, S. Senanayake, M.A. Barteau, ChemSusChem 1 (2008) 905.

[4] P.D. Vaidya, A.E. Rodrigues, Chem. Eng. J. 117 (2006) 39.
[5] A. Haryanto, S. Fernando, N. Murali, S. Adhikari, Energy Fuels 19 (2005) 2098.
[6] M. Ni, Y.C. Leung, M.K.H. Leung, Int. J. Hydrogen Energy 32 (2007) 3238.
[7] G. Kolb, Fuel Processing for Fuel Cells, Wiley-VCH, Weinheim, 2008, pp. 1–434.
[8] W. Ehrfeld, V. Hessel, H. Löwe, Microreactors: New Technology for Modern Chemistry, Wiley-VCH, Weinheim, 2000, pp. 1–283.
[9] F. Haga, T. Nakajima, H. Miya, S. Mishima, Catal. Lett. 48 (1997) 223.
[10] J. Llorca, N. Homs, J. Sales, P. Ramírez de la Piscina, J. Catal. 209 (2002) 306.
[11] J. Llorca, P. Ramírez de la Piscina, J.A. Dalmon, J. Sales, N. Homs, Appl. Catal., B 43 (2003) 355.
[12] J. Llorca, J.A. Dalmon, P. Ramírez de la Piscina, N. Homs, Appl. Catal., A 243 (2003) 261.
[13] S. Freni, S. Cavallaro, N. Mondello, L. Spadaro, F. Frustreri, Catal. Commun. 4 (2003) 259.
[14] F. Mariño, G. Baronetti, M. Jobbagy, M. Laborde, Appl. Catal., A 238 (2003) 41.
[15] J. Llorca, N. Homs, J. Sales, J.L.G. Fierro, P. Ramírez de la Piscina, J. Catal. 222 (2004) 470.
[16] J. Llorca, P. Ramírez de la Piscina, J.A. Dalmon, N. Homs, Chem. Mater. 16 (2004) 3573.
[17] J. Llorca, N. Homs, P. Ramírez de la Piscina, J. Catal. 227 (2004) 556.
[18] M.S. Batista, R.K.S. Santos, E.M. Assaf, J.M. Assaf, E.A. Ticianelli, J. Power Sources 134 (2004) 27.
[19] A. Kaddouri, C. Mazzocchia, Catal. Commun. 5 (2004) 339.
[20] H. Song, L. Zhang, R.B. Watson, D. Braden, U. Ozkan, Catal. Today 129 (2007) 346.
[21] J.A. Torres, J. Llorca, A. Casanovas, M. Domínguez, J. Salvadó, D. Montané, J. Power Sources 169 (2007) 158.
[22] M. Benito, R. Padilla, L. Rodríguez, J.L. Sanz, L. Daza, J. Power Sources 169 (2007) 167.
[23] S. Tutti, F. Pepe, Catal. Lett. 122 (2008) 196.
[24] H. Song, U. Ozkan, J. Catal. 261 (2009) 66.
[25] A. Casanovas, C. de Leitenburg, A. Trovarelli, J. Llorca, Catal. Today 138 (2008) 187.
[26] A. Casanovas, M. Saint-Gerons, F. Griffon, J. Llorca, Int. J. Hydrogen Energy 33 (2008) 1827.
[27] J. Llorca, A. Casanovas, T. Trifonov, A. Rodríguez, R. Alcubilla, J. Catal. 255 (2008) 228.
[28] M. Domínguez, E. Taboada, E. Molins, J. Llorca, Catal. Today 138 (2008) 193.
[29] A. Casanovas, M. Domínguez, C. Ledesma, E. López, J. Llorca, Catal. Today 143 (2009) 32.
[30] R. Nedyalkova, A. Casanovas, J. Llorca, D. Montané, Int. J. Hydrogen Energy 34 (2009) 2591.
[31] A. Casanovas, C. de Leitenburg, A. Trovarelli, J. Llorca, Chem. Eng. J. 154 (2009) 267.
[32] E. López, A. Irigoyen, T. Trifonov, A. Rodríguez, J. Llorca, Int. J. Hydrogen Energy 35 (2010) 3472.
[33] A. Casanovas, M. Roig, C. de Leitenburg, A. Trovarelli, J. Llorca, Int. J. Hydrogen Energy 35 (2010) 7690.
[34] M. Domínguez, E. Taboada, H. Idriss, E. Molins, J. Llorca, J. Mater. Chem. 20 (2010) 4875.
[35] J.A. Dalmon, G.A. Martin, C.R. Acad. Sci. Paris Serie C 267 (1968) 610.
[36] G. Zhang, Y. Zhao, F. Tao, H. Li, J. Power Sources 191 (2006) 723.
[37] S. Petit, A. Decarreau, F. Martin, R. Buchet, Phys. Chem. Miner. 31 (2004) 585.
[38] R. Al-Oweini, H.J. El-Rassy, Mol. Struct. 919 (2009) 140.